

# Control of vibrations for a parallel manipulator with flexible links – concepts and experimental results

M Morlock<sup>1</sup>, M Burkhardt<sup>2</sup> and R Seifried<sup>1</sup>

<sup>1</sup> Institute of Mechanics and Ocean Engineering, Hamburg University of Technology,  
21073 Hamburg, Germany

<sup>2</sup> Institute of Engineering and Computational Mechanics, University of Stuttgart,  
70569 Stuttgart, Germany

E-mail: merlin.morlock@tuhh.de, robert.seifried@tuhh.de

**Abstract.** A comprehensive control approach is presented to reduce the vibrations of a parallel manipulator with a kinematic loop and two flexible links whereof the longer one can show significant oscillations. The control objectives are end-effector trajectory tracking and active vibration control. The system is modeled as a flexible multibody system and exact feedforward control based on the full dynamic flexible multibody system is applied to improve the end-effector trajectory tracking performance. Furthermore, the effect of different position control concepts for the two linear drives, such as gain scheduling for the utilized cascade control and a model based friction compensation, on the movers themselves as well as on the end-effector are discussed, which can be conflicting. Experimental results are presented illustrating the achievable accuracy of the end-effector tracking for different trajectories while showing significant error reductions for a feedforward control based on an elastic model in contrast to a rigid one. Finally, a model based curvature controller is utilized which actively controls the occurring oscillations of the parallel manipulator. Here, a proportional controller as well as a linear-quadratic regulator are applied and the impact of an additional curvature control on the end-effector tracking performance is investigated.

## 1. Introduction

Systems with flexible manipulators offer the potential of a significant decrease in energy as well as material consumption and smaller actuators [1]. Nevertheless, the reduced stiffness increases the end-effector trajectory tracking error. Additionally, such a tracking task of flexible multibody systems often involves difficulties as the system, due to the body flexibilities, possesses less control inputs than degrees of freedom. This does not allow to simply apply classical approaches known from fully actuated systems [2]. For these underactuated systems the body flexibilities need to be taken into account for designing controllers [3, 4].

An exact feedforward control approach for end-effector trajectory tracking based on full dynamic flexible multibody systems has been applied previously [5], which is further tested experimentally and extended by feedback within this research. In order to show the possible tracking performance a nonlinear parallel manipulator with a highly flexible link and a kinematic loop is considered, as sketched in Figure 1. It is investigated to what extent the concepts discussed in [6] concerning gain-scheduling and friction compensation for the actuators improve



the mover position control and the corresponding effect on the end-effector trajectory tracking. This yields first experimental results on the accuracy of the offline trajectory planning of the feedforward control, based on an elastic model, for well tuned actuator controls. Nevertheless, the performance limitation of a pure feedforward control caused by unmodeled effects can be observed. Moreover, it is confirmed that the tracking error is typically significantly better when compared to a case with a rigid model for the feedforward control, in the case of trajectories in which large oscillations are excited. Finally, the curvature controller developed in [6] is extended with a linear-quadratic regulator (LQR) approach and used for curvature trajectory tracking. Experiments show that for a case of imprecise feedforward control a curvature controller can significantly improve the end-effector trajectory tracking performance although no end-effector position feedback is utilized.

## 2. Experimental procedure

In order to test the developed control concepts for flexible multibody systems, several experiments are presented throughout this research. This section serves to explain the corresponding experimental procedure.

### 2.1. Experimental setup

The considered experimental setup is illustrated in Figure 1 and a photo as well as details on the setup can be found in [5]. As pointed out in [6] two thin elastic links, connected by a revolute joint, are mounted on two identical and parallel linear drives with two additional revolute joints, which yields a so-called lambda kinematics. The longer link on the left can show significant oscillation amplitudes in the  $xy$ -plane in contrast to the short link on the right, which only exhibits negligible vibrations and is therefore approximated as a rigid body. Note that  $xyz$  is an inertial coordinate system and  $s_1$  and  $s_2$  are the mover positions from the center of the linear drives acting in the range of motion of  $s_1, s_2 \in [-0.3 \text{ m}, 0.3 \text{ m}]$ . The corresponding angles are denoted as  $\alpha_1$  and  $\alpha_2$ . Within this research, the numbers 1 and 2 in an index identify the related mover. Besides, at the end of the longer arm an end-effector mass with two reflective markers is added for video tracking.

Four strain gauges are used in a Wheatstone bridge circuit in order to obtain the curvature of the long link at a significant point. As curvature trajectory tracking is intended in Section 4 the strain gauges need to be calibrated accurately. The gain of the measurement amplifier is obtained with a so-called additive calibration signal. Based on this information, the curvature  $\kappa$

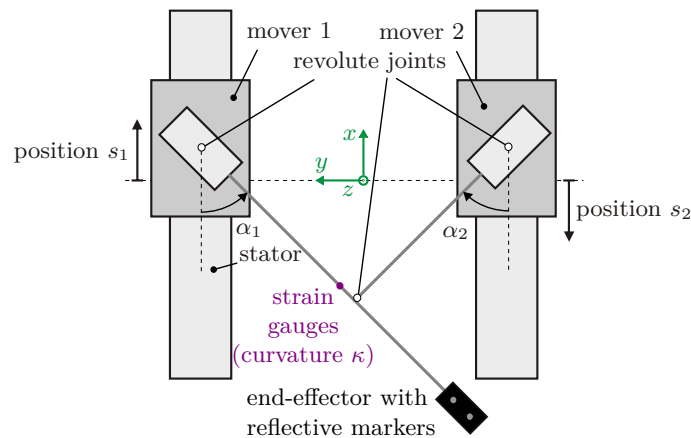


**Figure 1.** Sketch of the experimental setup.

can be calculated with the relationship between curvature and strain  $\epsilon$ , see [7], and the formula for a bending beam presented in [8], leading to

$$\kappa = -\epsilon/d_n = -\frac{U_o}{kd_n U_i}. \quad (1)$$

Here,  $U_o$  is the bridge output voltage and  $U_i$  denotes the bridge input or excitation voltage. The term  $k$  is the gauge factor of the strain gauges and  $d_n$  denotes the signed distance from the neutral beam axis. Note that the sign of the curvature  $\kappa$  is positive when there is compression at the strain gauges on the right-hand side of the long link considered in the position in Figure 1. Tests show that the measured and modeled curvatures fit well, building the basis for the curvature controller presented in Section 4.

## 2.2. Video tracking

In order to measure the trajectory tracking performance of the end-effector, video tracking is utilized. Here, a UI-3060CP camera is mounted vertically over the experimental setup, recording the two reflective markers on the end-effector within an area of interest of the  $xy$ -plane. The camera is used with 100 frames per second (FPS) for line trajectories of the end-effector and 70 FPS for ellipse trajectories (see Figure 3) as the computational load is higher for the larger area of interest for the ellipse at the same zoom. The change in FPS does not result in noticeable differences within the image processing. More important is utilizing a small exposure time such as the chosen 3.5 ms to keep the motion blur small. Especially for the ellipse the markers can thus be well separated for motions in the longitudinal direction of the long link. Moreover, measurements are done with a light source that shows no flickering which is mounted close to the camera in a low light setting. This improves the contrast between the points to track and the background.

The utilized offline image processing algorithm is based on [5]. To obtain reasonable results, reference video measurements are necessary to identify on the one hand an accurate value for the rotation of the camera relative to the inertial coordinate system. On the other hand, for the conversion from pixels to meters the distance in meters between the two points needs to be found which are identified as the marker positions by calculating the expected values. In this regard, the end-effector is moved and held at the end position until the position error is negligible. Then, the rotation matrix and the marker distance are obtained by fitting the measured to the theoretical end point. For the considered measurements the conversion factor of the video images to millimeters is approximately 0.33 mm/pixel. Note that the translation is simply obtained by setting the initial measured values in steady-state on the theoretical start values of the considered trajectory, assuming zero position error. This is justified by typically having a negligible starting position error. Besides, the end-effector positions extracted from the camera measurements are interpolated with a cubic spline.

As there was no direct way for synchronizing the video with the trajectory start, the time offset is determined at the instance when a motion of 2 mm is detected for the end-effector in the video and the simulation. Here, it is assumed that for the smooth trajectory starts differences between measurement and simulation are small.

## 2.3. Control structure

In Figure 2 the overall control structure is illustrated which holds for both linear drives. Here, a cascade controller is used for both movers being helpful in the presence of disturbances [9], especially when significant oscillations of the long elastic arm occur. Moreover, precomputed feedforward signals can be directly used for the position, velocity and current. The friction compensation based on the Stribeck model [10] and the gain scheduling introduced in [6] are applied, which have shown to further improve the control performance. Here, the gains  $P_p$  and

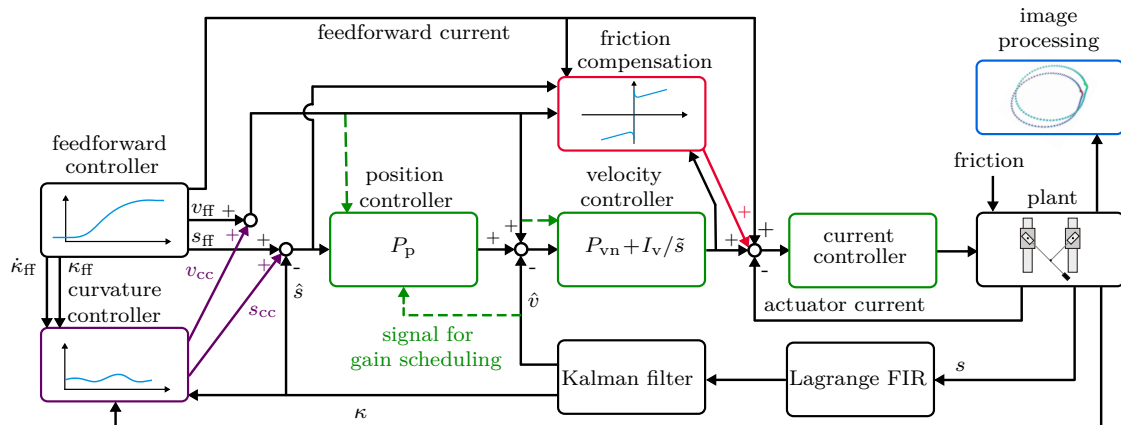


**Figure 2.** Overall control structure.

$I_v$  are scheduled in contrast to  $P_{vn}$  which is kept constant. The signal indices “cc” and “ff” stand for curvature control and feedforward control, respectively. The variable  $\tilde{s}$  denotes the complex frequency parameter of the Laplace transform,  $s$  are the mover positions,  $v$  the mover velocities and the hat symbol represents filtered and estimated quantities, respectively. For more details it is referred to [6].

In the following four cases of control settings are tested which are given in Table 1. These are denoted as case 1 to 4 throughout this research. Note that the index “n” within the controller parameters denotes the nominal value which is actually applied or used as a basis for gain scheduling.

**Table 1.** Controller cases.

Case	gain scheduling	friction compensation	cascade control gains			feedforward model
			$P_{pn}$ [Hz]	$P_{vn}$ [As/m]	$I_{vn}$ [A/m]	
1	yes	yes	18.33	5	400	elastic
2	no	no	18.33	5	400	elastic
3	no	no	10	3	10	elastic
4	yes	yes	18.33	5	400	rigid

### 3. Feedforward control

In order to obtain an improved end-effector tracking performance, a feedforward controller is designed based on the full dynamic flexible model of the manipulator which plans the trajectories of all states offline.

#### 3.1. Feedforward control based on exact model inversion

The following description of the feedforward controller design is based on [5], where more details are provided. The flexible multibody system is described using the floating frame of reference approach [11]. Due to the kinematic loop of the considered system, the equations of motion are stated in terms of the dependent coordinates  $z$  which consist of the drive positions  $s_1$  and  $s_2$ , the two angles  $\alpha_1$  and  $\alpha_2$  as well as of the elastic coordinates  $q_e$  of the long link. The forward

dynamics of the flexible multibody system can then be described by a set of differential-algebraic equations

$$\mathbf{M}(\mathbf{z})\ddot{\mathbf{z}} = \mathbf{f}(\mathbf{z}, \dot{\mathbf{z}}) + \mathbf{B}(\mathbf{z})\mathbf{u} + \mathbf{C}(\mathbf{z})^T\boldsymbol{\lambda}, \quad (2a)$$

$$\mathbf{0} = \mathbf{c}(\mathbf{z}). \quad (2b)$$

Here,  $\mathbf{c}$  are constraint equations for the kinematic loop and  $\boldsymbol{\lambda}$  are the corresponding Lagrange multipliers. Moreover,  $\mathbf{M}$  is the generalized mass matrix,  $\mathbf{f}$  is the generalized force vector containing the centrifugal, Coriolis and gyroscopic forces as well as applied forces which are not related to the control inputs  $\mathbf{u}$ . The Jacobian-matrix of the constraints is denoted by  $\mathbf{C}$  and  $\mathbf{B}$  is the input matrix of the controls. Note that bold capital letters denote matrices, bold uncapitalized letters represent vectors and letters which are not bold are scalars.

The long elastic link is modeled with the linear finite element method and reduced with a hybrid model-order reduction, combining the Craig-Bampton approach with Gramian-matrix-based reduction techniques [12], resulting in six elastic coordinates.

Now, the inverse dynamics can be obtained by extending the forward dynamics of (2) by additional servo-constraint equations [3, 13]

$$\mathbf{0} = \boldsymbol{\varsigma}(t, \mathbf{z}), \quad (3)$$

which describe the trajectory tracking problem. The control inputs  $\mathbf{u}$  are used to enforce these servo-constraints. The feedforward control is then obtained by the solution of the differential-algebraic equations consisting of (2) and (3). In accordance with nonlinear control theory the remaining dynamics of the inverse model is denoted as internal dynamics [14]. As the considered internal dynamics is unstable when using the end-effector point as output, a two-point boundary value problem needs to be solved in order to obtain a bounded solution [15]. With the desired trajectory of the end-effector, the trajectories for the dependent coordinates  $\mathbf{z}(t)$  and their time derivatives as well as the trajectories for the input signals  $\mathbf{u}(t)$  can be precalculated offline.

This trajectory planning will be used as the so-called elastic feedforward control in order to improve the end-effector trajectory tracking performance. A so-called rigid feedforward control is also used for comparison at which an equivalent rigid model is used. This can be solved algebraically using classical inverse kinematics and inverse dynamics [16].

### 3.2. Experiments based on feedforward trajectories for the actuators

In order to show the accurateness of the introduced feedforward control, the precalculated mover trajectories for the position, velocity and current are applied to the corresponding loops of the cascade controller, see Figure 2, without any curvature feedback.

Two desired end-effector trajectories, a line and an ellipse, are used to benchmark the tracking performance. The desired paths in the  $xy$ -plane are illustrated in Figure 3 along with results of the video tracking. The line starts at  $x = -0.6$  m,  $y = -0.5$  m and the ellipse starts and ends at  $x = -0.8$  m,  $y = -0.3$  m. The times written after line and ellipse denote the time between a trajectory start and end. Great improvement can be observed when using an elastic instead of a rigid feedforward control, leading to a reduction of the tracking error but also of unwanted oscillations which are present e.g. at the trajectory end. The significant overshoots in the paths for the rigid feedforward control are mainly due to motions transverse to the longitudinal axis of the long link which induce a bending. For the line the motion is primarily transverse to this axis and for the ellipse the two largest deviations from the path occur also when the motion includes an essential transverse part. Furthermore, in the rigid case for the faster line trajectory the flexibility of the link causes severe deviations from the desired path right from the start and higher maximum deviations compared to the ellipse. Besides, the marks in path plots within the current research denote the end-effector point of the individual frames captured by the camera.

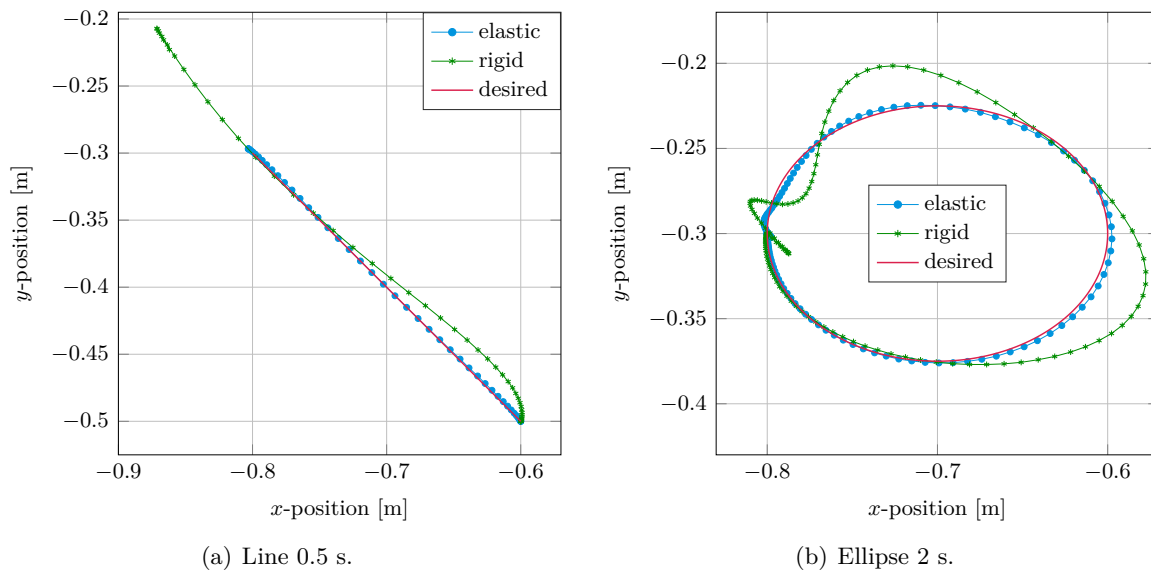


**Figure 3.** Desired and measured end-effector paths describing a line (in 0.5 s) and an ellipse (in 2 s) for an elastic (case 1) and a rigid (case 4) feedforward controller.

Thus, from a larger distance between two successive points a higher end-effector velocity can be inferred.

In Figure 4 the root mean square error  $e_{\text{rms}}$  and the maximum error  $e_{\text{max}}$  of the end-effector trajectory tracking experiments are illustrated, for the four controller cases summarized in Table 1. Here and in all following charts each bar represents the average of three measurements. Above all, the potential of an elastic feedforward control is again recognizable when comparing cases 1 and 4 with the same cascade controller, especially for trajectories with large oscillations in a rigid feedforward case such as the line within 0.5 s and the ellipse within 2 s. For those trajectories, the end-effector tracking error is even significantly smaller for case 3, with a badly tuned cascade controller, compared to the rigid feedforward case. Furthermore, as expected the slow line in 2 s shows much smaller errors than its faster version for the individual cases. Additionally, it should be noted that the rigid case 4 is better than the elastic case 3 and is close to the better tuned elastic feedforward cases 1 and 2. This clearly shows that for slow movements where no large oscillations are excited, a rigid feedforward control might be sufficient. Besides, the tracking error for the line 0.5 s for case 1 is much better than the elastic case in [5], since there the end-effector and the mover position accuracy are comparable with case 3. As this third case is always significantly worse than case 1, it is confirmed that the elastic feedforward control typically only shows its potential when combined with a well tuned feedback controller.

In Figure 6 the position errors of the movers are shown in order to investigate the influence of the mover accuracy on the end-effector tracking performance. Here, the applied friction compensation and gain scheduling lead to a significant improvement from case 2 to case 1, without risking the stability of the system. Theoretically, the improvement should almost directly translate onto the end-effector tracking accuracy. See the simulated end-effector trajectory errors when the measured mover trajectories are applied to the flexible model within Figure 5, at which the better mover performance of case 1 outperforms case 2. This is obviously not the case in the measured results shown in Figure 4, at which enhanced mover position errors may also deteriorate the results. Most likely, the major reason is that the modeling inaccuracies of the feedforward trajectories dominate, covering the effect of a better mover positioning on the end-effector tracking and leading to much higher errors for cases 1 and 2 in contrast to the

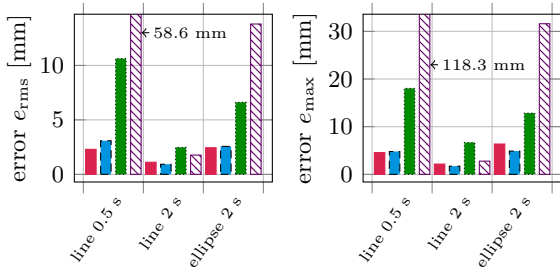


**Figure 4.** Video measurement end-effector trajectory errors for different trajectories and the elastic feedforward case 1 (■), case 2 (■), case 3 (■) as well as the rigid feedforward case 4 (▨).

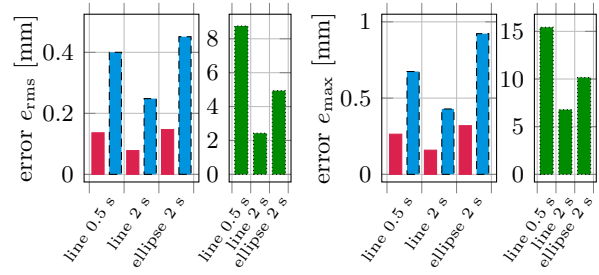


**Figure 5.** Simulated end-effector trajectory errors for measured mover trajectories applied to the flexible model for the elastic feedforward case 1 (■), case 2 (■) and case 3 (■).

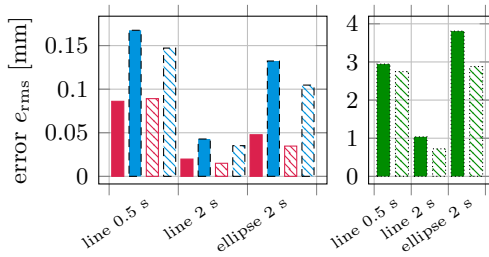
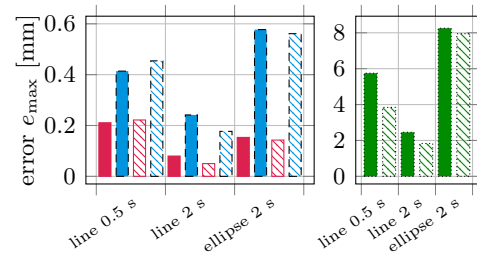


**Figure 6.** Mover trajectory errors for the elastic feedforward case 1, mover 1 (■) and 2 (▨), case 2, mover 1 (■) and 2 (▨) as well as case 3, mover 1 (■) and 2 (▨).



simulation results. Moreover, inaccuracies of the utilized video tracking technique add to this. Consequently, the mover positioning error in case 1 is accurate enough to only have a minor influence on the end-effector tracking error in contrast to [5], at which a mover control similar to case 3 was used. Also, Figure 5 confirms that a further improvement of the mover control has an insignificant potential for the experimental end-effector tracking performance. Thus, future research needs to account for end-effector tracking errors e.g. with a type of end-effector feedback control.

#### 4. Curvature control

As a next step, a curvature controller is used in order to investigate if positive effects on the end-effector error are to be expected with an additional curvature trajectory tracking for the curvature  $\kappa$  of the long link. The oscillations of this highly flexible link are now actively controlled with an online change of the feedforward mover trajectories. Applying the curvature controller to end-effector trajectory tracking extends [6, 17] and besides a proportional curvature controller also an LQR approach is introduced. Note that in this section, the focus is directed to the elastic feedforward trajectories according to case 1 since they outperformed the rigid ones.

##### 4.1. Curvature control concept

The control structure of the proposed curvature controller, which is based on [6, 17], is presented in Figure 7. Here, a band-pass filter is implemented to remove noise from the strain gauge signals and to eliminate offsets which arise even after sensor zeroing. Note that the filtering is kept small in order to avoid a significant signal alteration since the curvature is used for tracking. The main idea is to change the dynamics of the first eigenmode, which is clearly dominant, to obtain

a better curvature trajectory tracking performance. The movers are approximated as position actuators, justified by accurately controlled direct drives. Thus, only elastic degrees of freedom remain and the resulting equations of motion are linearized at 101 different mover position sums  $s_1 + s_2$ , since the constellation of the kinematics is identical for  $s_1 + s_2 = \text{constant}$ . Subsequently, the Cholesky decomposition is used for the mass matrix, a modal transformation is applied for an undamped version of the considered system and the off-diagonal damping terms are neglected based on the decoupling approximation [18]. As a result, one obtains the decoupled equation for the modal coordinate  $q_m$  of the first eigenmode as

$$\ddot{q}_m + d_m \dot{q}_m + k_m q_m = \mathbf{b}_m \mathbf{u}_m, \quad (4a)$$

$$\dot{\kappa} = c_m \dot{q}_m, \quad (4b)$$

with the damping  $d_m$  and stiffness  $k_m$ . The vector  $\mathbf{u}_m$  consists of the two mover accelerations  $a_1$  and  $a_2$ . When applying a QR decomposition to  $\mathbf{b}_m^T$  as shown in detail in [6], the input can be written as

$$\mathbf{u}_m = \begin{pmatrix} Q_{11} \\ Q_{21} \end{pmatrix} (u_{cc} + u_{ff}), \quad (5)$$

with  $Q_{11}$  and  $Q_{21}$  being elements from the decomposition. Here,  $u_{cc}$  and  $u_{ff}$  are inputs related to the curvature controller and the feedforward controller. The values of  $Q_{11}$  and  $Q_{21}$  at the different mover positions are illustrated in Figure 8. Here, the gain of the second mover is zero at  $s_1 + s_2 \approx 0.42$  m. The reason is that a motion of this mover does not influence the end-effector at the considered location, being a reversal point at which the end-effector changes the direction of motion for a monotonously changing  $s_2$ . This means that for an  $s_2$  moving towards the reversal point the long link gets pushed away until at the reversal the short link is parallel to the  $y$ -axis. A further change of  $s_2$  in the same direction then pulls on the long link causing the end-effector to change the direction of motion. Also, Figure 8 shows that both gains are limited within this approach.

As a next step, substituting the decomposed  $\mathbf{b}_m^T$  and (5) into (4a) gives

$$\ddot{q}_m + d_m \dot{q}_m + k_m q_m = r(u_{cc} + u_{ff}), \quad (6)$$

with  $r$  resulting from the QR decomposition. As the applied elastic feedforward controller inputs approximately the desired dynamics, one can write (6) in an ideal case as

$$\ddot{\tilde{q}}_m + d_m \dot{\tilde{q}}_m + k_m \tilde{q}_m = -r u_{cc}, \quad (7)$$

with  $\tilde{q}_m = q_{m,ff} - q_m$  and  $q_{m,ff}$  being the feedforward trajectory of the modal coordinate  $q_m$ . Subsequently, based on (4b) a proportional (P) controller of the form

$$u_{cc} = P_{cc}(\dot{\kappa}_{ff} - \dot{\kappa}) = P_{cc} c_m \dot{\tilde{q}}_m \quad (8)$$

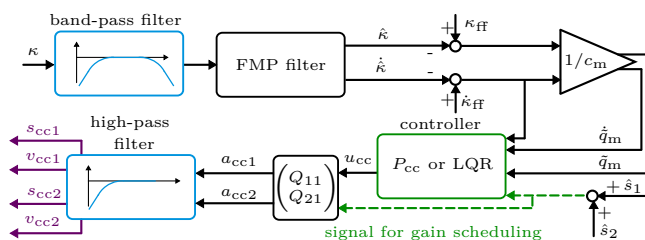


**Figure 7.** Curvature control structure with a proportional controller and an LQR.

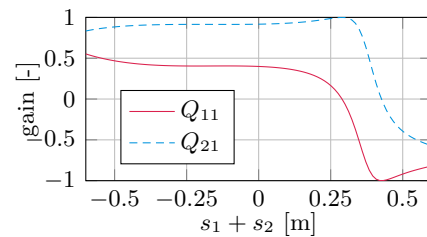


**Figure 8.** Gains for the distribution of the controller output to the mover accelerations.

is proposed, which yields

$$\ddot{q}_m + (d_m + rP_{cc}c_m)\dot{q}_m + k_m\tilde{q}_m = 0. \quad (9)$$

As  $d_m$ ,  $k_m$ ,  $c_m$  and  $r$  are positive,  $P_{cc} > 0$  leads to an increased damping of oscillations around the curvature trajectory and corrects inaccuracies of the feedforward control.

Next, an LQR is designed which also takes curvature tracking errors into account. This is contrary to the previous approach which only uses the corresponding time derivative. A state space representation of (7) is

$$\dot{\mathbf{x}}_{lqr} = \begin{pmatrix} 0 & 1 \\ -k_m & -d_m \end{pmatrix} \mathbf{x}_{lqr} + \begin{pmatrix} 0 \\ -r \end{pmatrix} u_{cc}, \quad (10a)$$

$$(10b)$$

with  $\mathbf{x}_{lqr} = (\tilde{q}_m \ \dot{\tilde{q}}_m)^T$  and  $u_{cc} = -\mathbf{k}_{lqr}^T \mathbf{x}_{lqr}$  at which  $\mathbf{k}_{lqr}$  contains the LQR gains. These gains change with a differing  $s_1 + s_2$ . In order to remove position and velocity drift of the movers, the calculated mover accelerations  $a_{cc1}$  and  $a_{cc2}$  from the curvature controller are filtered with a high-pass filter given in [6] and the filtered positions and velocities are added to the feedforward trajectories.

#### 4.2. Experimental results

First experimental results are now presented for a curvature trajectory tracking in combination with the mover trajectory tracking. The weighting matrix of the states for the LQR design is based on the approach described in [19], at which the inverse of the maximum squared states is chosen for the corresponding diagonal elements. Off-diagonal terms are set to zero. The weighting for the input is tuned to obtain similar maximum mover position corrections as with the proportional curvature controller  $P_{cc} = 1 \text{ m}^2/\text{s}$  for the line trajectories and for the ellipse an LQR which is more aggressive than this P control is used. The gains within  $\mathbf{k}_{lqr}$  are solely negative. Moreover, since only well tuned cascade controllers are utilized (see Table 1, case 1), the assumption of position actuators is supported.

First, a case is considered with an additional load of 0.4 kg mounted close to the end-effector point, representing a model uncertainty which is neither included in the feedforward trajectory calculation nor in the curvature controller design. Thereby, it shall be investigated if a curvature controller can reduce the occurring end-effector trajectory tracking deviations. In Figure 9 results are shown for a desired line. Here, one can see that the additional load highly increases the overshoot at the end point of the path compared to the elastic case of Figure 3(a), which is however reduced when a proportional curvature controller is applied. This behavior is confirmed in Figure 10 at which the two different curvature controllers reduce the overshoot and the extreme values of the curvature. Note that the actual trajectories start at  $t = 1 \text{ s}$ . Furthermore, it can be observed that the end-effector drags behind at the beginning for an increased mass and also that the curvature tracking is improved by both controllers. Especially after the desired motion it can be seen that the curvature controllers significantly reduce the oscillations of the lightly damped system, since the damping is increased by up to two orders of magnitude and depending on the mover positions it is close to critical damping. Moreover, both controllers perform similar with the LQR showing a somewhat better end-effector tracking performance.

Note that the corrective motion  $s_{cc}$  of the curvature controllers at the start of Figure 10 basically moves the end-effector first in the direction of bending, decreasing the curvature amplitude. A similar behavior can be observed when regulating a constant point and e.g. hitting the end-effector with a stick transverse to the longitudinal axis of the link. Here, a curvature controller adds compliance by moving the end-effector approximately in the direction of impact, which finally reduces the oscillations.

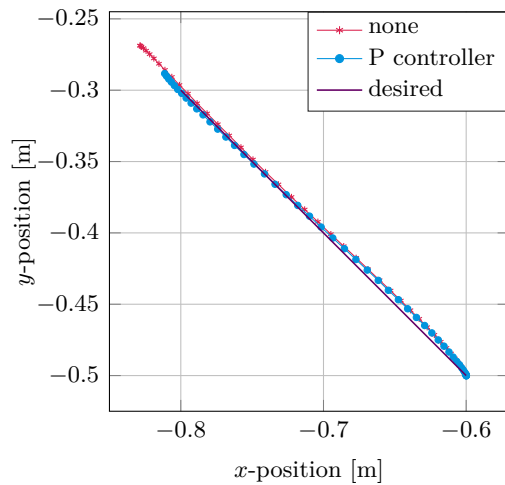


**Figure 9.** Desired and measured end-effector paths without a curvature controller and with a P curvature controller, for the line 0.5 s trajectory with an additional load of 0.4 kg and an elastic feedforward control.

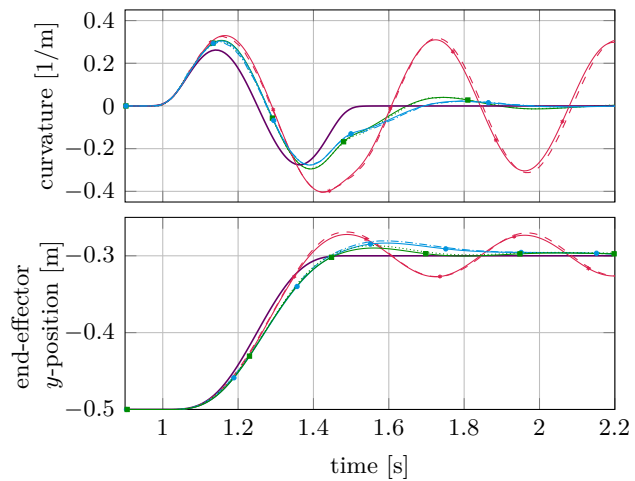


**Figure 10.** Results for the line 0.5 s trajectory with 0.4 kg additional load and an elastic feedforward control, showing the desired trajectory (—), a case without a curvature controller, measured (---) and simulated (---\*), a case with a P curvature controller, measured (---) and simulated (—) as well as a case with an LQR curvature controller, measured (.....) and simulated (---).

Besides, the simulated results in Figure 10 show that the model behaves pretty similar to the measurements. Differences arise from modeling inaccuracies such as having perfect strain gauge signals which are not filtered and perfect mover positioning in the simulations. Note that the  $x$ -position of the end-effector is not shown as it corresponds to the behavior of the  $y$ -coordinate.

Subsequently, measurements are conducted with three different curvature control settings, see Figure 11. Note that for the cases without a curvature controller, the results vary slightly when compared to Figure 4, amongst others as the cascade controller performance is not constant over time. Thus, for direct comparison to the cases with a curvature controller, new measurement sets are recorded.

Figure 11 demonstrates that the curvature controllers can help to improve the root mean square error even for the elastic cases without an additional load, but at the expense of the maximum error which increases slightly. Also, the more aggressive LQR which yields a better curvature tracking for the ellipse when compared to the P control, results in a worse end-effector trajectory tracking. Consequently, both aims can be conflicting. Nevertheless, both curvature controllers smoothen the trajectory ending of the ellipse by reducing the oscillations. For the case with an additional load, a great improvement can be seen for the maximum error which is due to the reduced overshoot at the trajectory end. Thus, a curvature controller can be advantageous if the load is uncertain. Besides, in most cases the P controller and the LQR perform similar.

From these results, it can be concluded that the curvature controller can indeed improve the trajectory tracking performance of the end-effector but can also lead to a deterioration since curvature and not end-effector tracking is the control objective of the curvature controller. The presented results depend on the specific trajectories as well as on the specific experimental setup. Also, in cases with small absolute errors such as the trajectories without an additional load, the measurement accuracy might have a non-negligible influence. Nevertheless, using a curvature

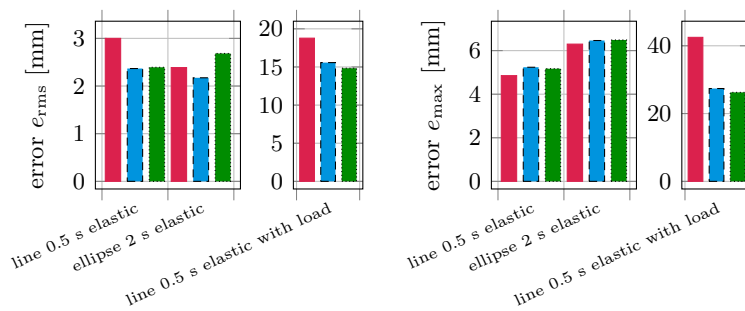


**Figure 11.** Video measurement end-effector trajectory errors for different trajectories or an additional load of 0.4 kg without a curvature controller (red), with a curvature controller realized as a P controller (blue) and as an LQR (green).

controller after the tracking task typically helps to reach the steady state for the curvature and mover positions faster. Especially in the case of large oscillations a curvature controller is helpful for a good mover positioning, as these oscillations are transferred to the movers.

Besides, simulations have been done with curvature controllers for rigid feedforward versions of the considered trajectories without an additional load. The performance turns out to be significantly worse compared to the elastic feedforward control and can even be deteriorated by a curvature control, which confirms the usefulness of an accurate feedforward control based on an elastic model.

## 5. Conclusions

A feedforward control concept for end-effector trajectory tracking for a multibody system with a highly flexible link and a kinematic loop is presented and investigated experimentally. First, only precomputed trajectories for the actuators are applied in order to perform end-effector trajectory tracking. Significant advantages can be observed for an elastic feedforward control, in contrast to a rigid one, for trajectories at which large oscillations are excited. By improving the actuator position control, the experimental limits of the end-effector trajectory tracking performance are reached for the applied feedforward control.

Afterwards, a model based curvature controller is added, changing the precomputed trajectories of the direct drives to actively reduce deviations from the precomputed curvature trajectory. A proportional and an LQR curvature controller are tested showing similar results in most cases. For inaccurate feedforward trajectories for the movers, a curvature controller can be very helpful. However, in general the curvature controller does not necessarily improve the end-effector trajectory tracking. Consequently, a type of feedback of the end-effector position is required to further enhance the tracking results.

## Acknowledgments

The authors would like to thank the German Research Foundation (DFG) for their financial support of the project SE1685/3-2 and Professor Peter Eberhard for providing the experimental setup at the Institute of Engineering and Computational Mechanics at the University of Stuttgart.

## References

- [1] Tokhi M O and Azad A K (eds) 2008 *Flexible Robot Manipulators: Modelling, Simulation and Control* vol 68 (London: IET)
- [2] Seifried R, Burkhardt M, Morlock M and Eberhard P 2015 *ECCOMAS Thematic Conf. on Multibody Dynamics, Barcelona, Spain*
- [3] Seifried R 2014 *Dynamics of Underactuated Multibody Systems* (Springer)
- [4] Luca A D and Book W 2008 *Handbook of Robotics – Chapter 13* (Berlin Heidelberg: Springer)
- [5] Burkhardt M, Seifried R and Eberhard P 2015 *J. of Mechanical Science and Technology* **29** 2685–91

- [6] Morlock M B, Burkhardt M and Seifried R 2015 *IEEE/RSJ Int. Conf. on Intelligent Robots and Systems* (IEEE) pp 2354–59
- [7] Craig R R and Kurdila A J 2006 *Fundamentals of Structural Dynamics - Section 12.2* (Hoboken: John Wiley & Sons)
- [8] Hoffmann K 2001 *technical articles of Hottinger Baldwin Messtechnik, S1569-1.1 en, Darmstadt, Germany*
- [9] Kaya I, Tan N and Atherton D 2005 *44th IEEE Conf. on Decision and Control and European Control Conference* (IEEE) pp 3055–60
- [10] Olsson H, Åström K J, Canudas-De-Wit C, Gäfvert M and Lischinsky P 1998 *European J. of Control* **4** 176–95
- [11] Shabana A A 1997 *Multibody System Dynamics* **1** 189–222
- [12] Burkhardt M, Holzwarth P and Seifried R 2013 *Proc. of the 11th Int. Conf. on Vibration Problems, Lisbon, Portugal* ed Dimitrovová Z et al
- [13] Blajer W and Kołodziejczyk K 2004 *Multibody System Dynamics* **11** 343–64
- [14] Isidori A 1995 *Nonlinear Control Systems* 3rd ed (London: Springer)
- [15] Seifried R, Burkhardt M and Held A 2013 *Multibody Dynamics: Computational Methods and Applications, Computational Methods in Applied Sciences* vol 28 ed Samin J and Fisette P (Springer) pp 53–75
- [16] Ast A and Eberhard P 2006 *Archive of Applied Mechanics* **76** 181–97
- [17] Burkhardt M, Morlock M, Seifried R and Eberhard P 2015 *PAMM* **15** 49–50
- [18] Morzfeld M, Ma F and Ajavakom N 2008 *J. of Vibration and Control* **14** 1869–84
- [19] Hendricks E, Jannerup O and Sørensen P H 2008 *Linear Systems Control: Deterministic and Stochastic Methods - Section 5.4* (Berlin Heidelberg: Springer)